Development of Smart BZT-Cement Mortar Nanocomposites

Hamza M. Kamal
Materials Engineering Department, Mustansiriyah University, Baghdad, Iraq
dr.hamza.m.k@uomustansiriyah.edu.iq

Mohammed J. Kadhim
Materials Engineering Department, Mustansiriyah University, Baghdad, Iraq
dr.mohammed.j.k@uomustansiriyah.edu.iq

Layla M. Hasan
Materials Engineering Department, Mustansiriyah University, Baghdad, Iraq
laylamhasan@uomustansiriyah.edu.iq (corresponding author)

Received: 31 July 2025 | Revised: 27 September 2025 | Accepted: 5 October 2025

 DOI: https://doi.org/10.48084/etasr.13758

ABSTRACT

Nano Silica Fume (NSF) is characterized by its ultrafine particle size and high pozzolanic reactivity, and it has shown great potential in enhancing the structural and functional properties of cement-based materials. In this work, NSF was incorporated into Barium-Zirconate-Titanate (BZT) cement composites to assess its influence on the dielectric, piezoelectric, and mechanical behavior of the system. The microstructural examinations revealed that the NSF addition refined the internal morphology, improved the BZT particle dispersion, and stimulated the formation of additional Calcium Silicate Hydrate (C-S-H), resulting in a denser and more uniform matrix. The dielectric measurements indicated a notable increase in relative permittivity and a reduction in dielectric loss, primarily attributed to the improved BZT interconnectivity and interfacial polarization. The incorporation of NSF also enhanced the matrix-filler bonding and electromechanical coupling, leading to higher piezoelectric coefficients and better acoustic impedance. It additionally caused a significant improvement in the compressive strength of the cement mortar compared to the unmodified BZT-cement composite. The findings indicate that NSF functions simultaneously as a microstructure modifier and a performance enhancer, thus broadening the application of BZT-cement composites for multifunctional sensing and structural health monitoring purposes.

Keywords-Nano Silica Fume (NSF); BZT-cement composite; dielectric properties; piezoelectric behavior; microstructure; compressive strength

I. INTRODUCTION

In advanced structural technologies, piezoelectric actuators and sensors have attracted considerable attention for the development of a new generation of piezoceramic cement composites suitable for intelligent concrete structures [1]. Severe vibrations, such as those induced by earthquakes or strong winds, often cause substantial damage, posing significant risks to both human safety and structural integrity [2]. Consequently, the integration of smart devices, including sensors, transducers, and actuators, into building structures is an effective approach to mitigate such risks [3]. Perovskite piezoceramics play a pivotal role in civil engineering applications, such as bridges, roads, pavements, tunnels, airports, and buildings, due to their exceptional dielectric and piezoelectric properties [4]. Among these, lead-free piezoelectric ceramics have emerged as promising alternatives to lead (Pb), zirconium (Zr), and titanium (Ti) PZT-based materials, owing to their favorable piezoelectric performance, environmental compatibility, and suitability for concrete structures [5, 6]. These considerations have driven the development of piezoelectric cement composites that meet the structural and functional requirements of primary civil engineering elements while closely matching the properties of the host material [7, 8].

Previous studies have demonstrated various strategies for enhancing the performance of cement-based piezoelectric composites. Authors in [9] prepared lead-free $Bi_{0.5}Na_{0.5}TiO_3$/Portland cement composites with ceramic volume fractions of 30-70 vol.%. The results indicated that increasing particle content improved the dielectric and piezoelectric behavior, with the highest piezoelectric voltage constant observed at 30 vol.%. The influence of graphene on silica-fume-modified cement was investigated in [10],

revealing improvements in both the piezoelectric and ferroelectric properties. Similarly, in [11], the effect of hydration time on white Portland cement was studied, finding that prolonged hydration enhanced the dielectric and piezoelectric performance. In [12], a ternary cement composite was fabricated incorporating Polyvinylidene Fluoride (PVDF) and PZT, demonstrating that the PVDF addition improved the piezoelectric properties and reduced the poling time. Authors in [13] fabricated connectivity BZT-cement composites with varying epoxy resin content of 0-7 vol.% and BZT fractions of 40-60 vol.%. The results indicated that the epoxy incorporation enhanced matrix densification, reduced porosity, and improved piezoelectric response, with the highest charge coefficient d_{33}=93 pC/N observed at 7 vol.% epoxy and 60 vol.% BZT. Similarly, authors in [14] embedded lead-free, complex-ion-doped KNLNTS ceramics into cement composites of 30-70 vol.%, achieving acoustic impedance closely matched to concrete and a notable increase in piezoelectric response from 8.40 to 24.15 pC/N, confirming their suitability for stress, strain, and micro-crack detection in advanced structural health monitoring applications.

Following the same framework, other works [15-17] on BZT–cement composites focused more on the dielectric and piezoelectric properties and less on their impact on the mechanical performance. On the other hand, studies on nano-silica incorporation in cement mortars have shown significant improvements in strength and microstructure, though the electrical and piezoelectric effects were generally not investigated [18, 19].

In the current study, these two approaches are combined for the first time through the incorporation of NSF into BZT-cement mortars. The NSF addition was demonstrated to enhance both the mechanical strength and dielectric and piezoelectric performance by promoting improved particle dispersion, matrix densification, and interfacial adhesion. This dual enhancement positions BZT-NSF cement mortars as a novel class of multifunctional materials suitable for sustainable smart infrastructure and structural health monitoring applications.

II. MATERIALS AND METHODS

A. Preparation of BZT Piezoelectric Ceramics

BZT ceramics with the composition $BaZr_{0.05}Ti_{0.95}O_3$ were synthesized using the conventional ceramic fabrication procedure. The precursor oxide powders, supplied by Fluka Chemie GmbH with a purity of 99%, were weighed according to the stoichiometric ratios and thoroughly mixed. The resulting powder was milled with 2 wt.% polyvinyl alcohol (PVA) binder and then uniaxially pressed into pellets. The green pellets were dried and calcined at 1150 °C, followed by sintering at 1450 °C to obtain dense BZT ceramics.

B. Preparation of Cement Nano-Composites

Ordinary Portland Cement (OPC) (Table I) supplied by the Tasloga Cement Plant, Iraq, conforming to Iraqi Specification No. 5/1984, was used in all mixtures. The fine aggregate was sand (Table II) obtained from the Al-Akhdar area, Karbala Governorate, Iraq, with a maximum grain size below 5 mm and in compliance with the Iraqi Specification No. 45/1984. The mix proportion was maintained at a cement-to-sand ratio of 1:2.75, with a water-to-cement (W/C) ratio of 0.35. NSF (Table III) with an average particle size of 75 nm was used as a partial cement replacement at weight fractions of 1, 2, 4, and 6 wt.%.

TABLE I. MAIN OXIDE COMPONENTS OF OPC

Composition	Content (%)	Iraqi Specification No.5/1984
SiO_2	20.26	-
Al_2O_3	5.50	-
Fe_2O_3	2.19	-
CaO	61.39	-
MgO	2.29	< 5.00
SO_3	2.5	< 2.8
Free CaO	1.12	-
Loss on Ignition	3.4	< 4.00
Insoluble Residue	0.71	< 1.50

TABLE II. SAND GRADING AND REQUIREMENTS

Sieve size (mm)	Accumulative passing (%)	Limit of Iraqi specification No.45/1984
4.75	100	90-100
2.36	100	85-100
1.18	87.22	75-100
0.6	67.85	60-79
0.3	28.53	12-40

TABLE III. NSF CHEMICAL COMPOSITION

Chemical composition	Contents (%)
SiO_2	94
Al_2O_3	0.52
Fe_2O_3	0.87
CaO	0.53
MgO	1.23
Na_2O	0.41
K_2O	1.23
Loss on Ignition	1.2

To prepare the nano-composites, NSF was first dispersed in water at room temperature using magnetic stirring for 15 min to form a uniform colloidal suspension, which was then added to the cement and sand to form the mortar. The fresh mixture was cast into molds, demolded after 24 hours, and cured for 28 days under controlled conditions.

III. RESULTS AND DATA ANALYSIS

A. Microstructural Analysis

The microstructure of BZT ceramics sintered at 1450 °C was observed (Figure 1) under Scanning Electron Microscopy (SEM) at various magnifications. Two distinct grain sizes were revealed: large and small grains with well-defined cubic perovskite crystals, confirming the formation of BZT.

SEM micrographs of cement mortars without NSF (Figure 2) and with NSF (Figure 3) were compared, and it was revealed that the microstructure of plain cement mortar exhibits calcium silicate hydrate C-S-H gel that provides most of the mechanical strength and large hexagonal portlandite CH crystals, which are less desirable due to their lower strength and durability.

Capillary pores, caused by incomplete hydration, contribute to a coarse microstructure.

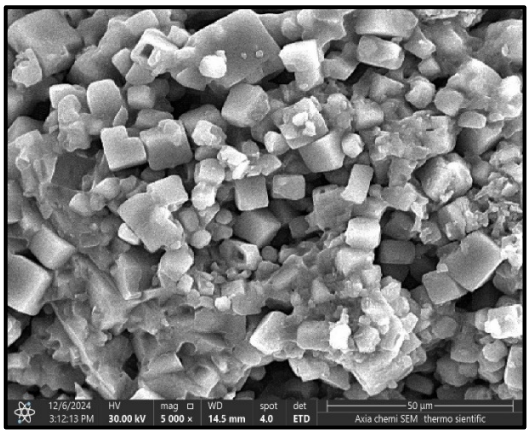

Fig. 1. BZT microstructure sintered at 1450 ºC.

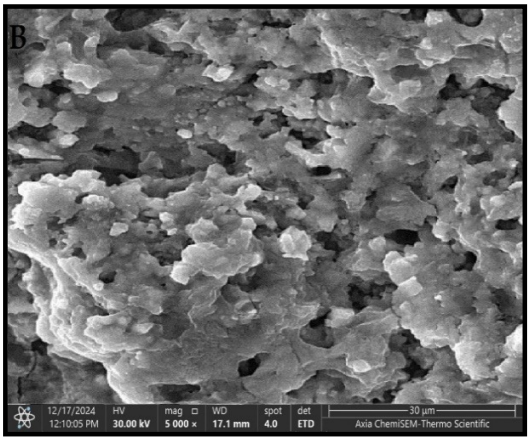

Fig. 2. Cement mortar microstructure without NSF.

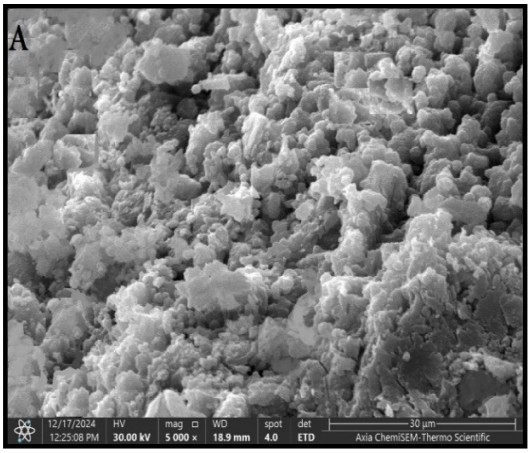

Fig. 3. Cement mortar microstructure with (4%) NSF.

In contrast, the addition of NSF refines the pore structure due to its filler effect, occupying microvoids and reducing capillary porosity. Moreover, NSF reacts pozzolanically with CH to form additional C-S-H gel [20], thereby consuming CH and densifying the matrix. NSF also promotes a more uniform distribution of hydration products by serving as a nucleation site that accelerates hydration [21].

The microstructure of BZT-cement composites with NSF (Figure 4) and without NSF (Figure 5) was compared. The BZT particles without NFS tend to agglomerate and show weak bonding with the surrounding matrix, leading to voids and limited load transfer. With NSF, particle dispersion and interfacial bonding significantly improve, resulting in better packing, reduced porosity, and stronger adhesion between the BZT particles and the cement matrix due to the additional C-S-H formed around the particles.

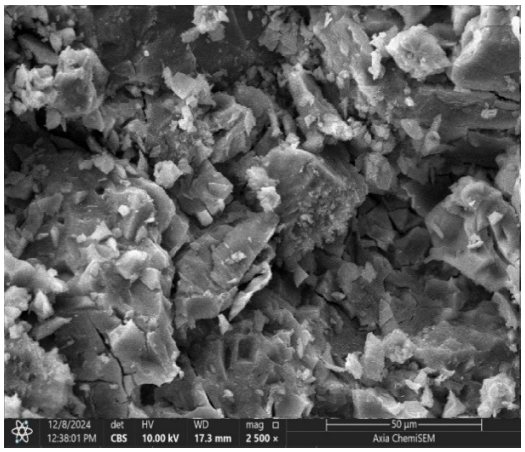

Fig. 4. BZT-cement composite microstructure without NSF.

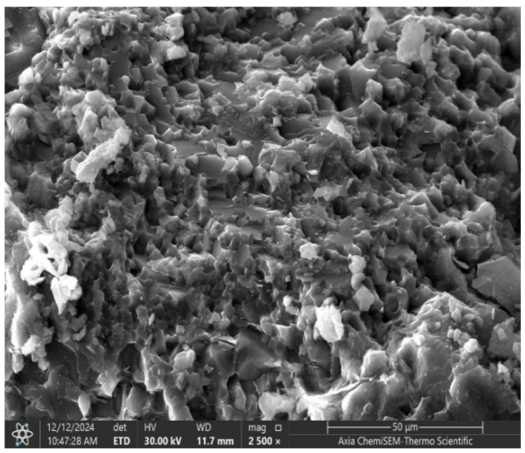

Fig. 5. BZT-cement composite microstructure with (4%) NSF.

B. Density Measurement

The effect of the NSF content on the density of cement mortars after 28 days of curing was measured (Figure 6) according to [22]. The density increased with an NSF addition up to 4 wt.%, before slightly decreasing at 6 wt.%, which results from the fine NSF particles filling voids within the matrix and enhancing packing density. The pozzolanic reaction of NSF also contributes to matrix densification and porosity reduction [23, 24]. The decrease beyond 4 wt.% is attributed to

nanoparticle agglomeration and increased water demand, which can create weak zones and reduce the overall density.

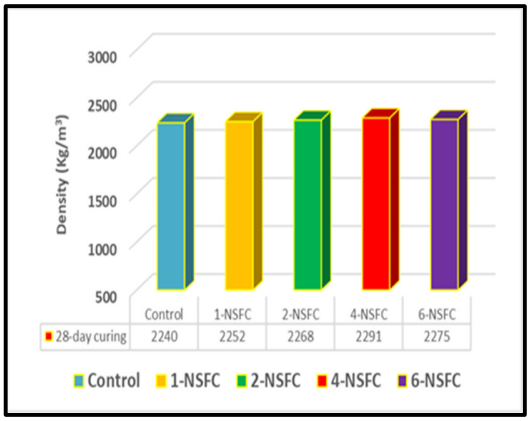

Fig. 6. Effect of different weight percentages of NSF on the density values of cement mortar.

C. Compressive Strength

The compressive strength was measured on 50×50×50 mm cubes after 28 days in accordance [25] using an ELE machine at a loading rate of 1.5 mmm/min. The NSF addition improved the compressive strength up to 4 wt.%, after which a slight decline occurred at 6 wt.% (Figure 7). This enhancement is attributed to the pozzolanic reaction of SiO_2 nanoparticles with calcium hydroxide to produce additional C-S-H gel, strengthening the cement matrix. At higher NSF contents, excessive surface area and agglomeration, due to strong van der Waals forces, increase the water demand and introduce weak points, reducing strength.

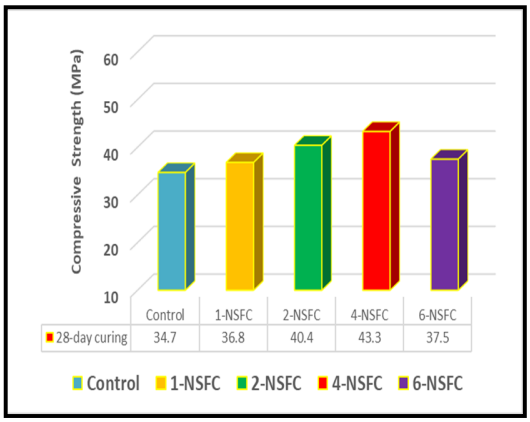

Fig. 7. Effect of different weight percentages of NSF on the performance of cement mortar in compressive strength.

The influence of BZT content on the compressive strength, with and without NSF was examined (Figure 8). Without NSF, the strength decreased with increasing BZT volume fraction due to the weak bonding and void formation around the ceramic particles. However, with 4 wt.% NSF, this reduction was mitigated, particularly at low BZT loadings. NSF enhances the Interfacial Transition Zone (ITZ), improving the load transfer and matrix cohesion.

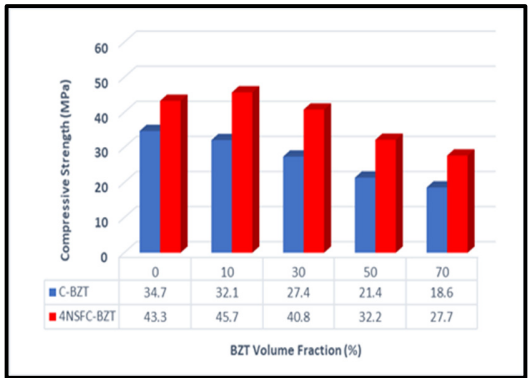

Fig. 8. Variation in compressive strength of BZT volume fractions with/without NSF.

D. Dielectric Properties

The dielectric behavior of the composites was examined in terms of the dielectric constant (Figure 9) and dielectric loss (Figure 10) at 1 kHz. The dielectric constant increased with BZT content due to the high intrinsic permittivity of BZT, which enhances the polarization within the composite. The dielectric loss also rose slightly with higher BZT loading, likely due to increased interfacial defects and energy dissipation under alternating electric fields.

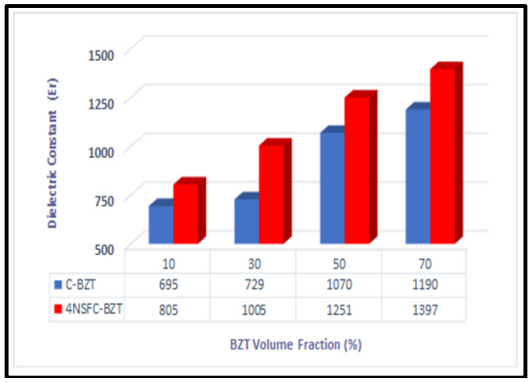

Fig. 9. Effect of BZT volume fractions on the dielectric constant of cement mortar with and without NSF.

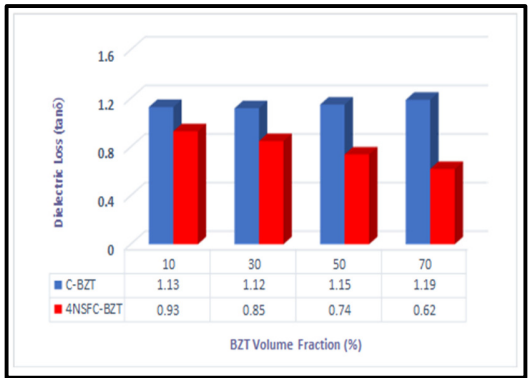

Fig. 10. Effect of BZT volume fractions on the dielectric loss of cement mortar with and without NSF.

The dielectric loss is also influenced by the moisture content and porosity of the mortar, which may be higher in the absence of NSF. When NSF was incorporated, both the dielectric constant and loss behavior improved. NSF enhanced the matrix homogeneity, particle dispersion, and interfacial bonding, which increased the dielectric constant while reducing the dielectric loss through porosity reduction and improved microstructural integrity.

E. Piezoelectric Properties

The incorporation of BZT markedly enhanced the piezoelectric response of the mortar [26]. The presence of NSF further increased the d_{33} values (Figure 11) by improving the uniformity and bonding of BZT particles, which facilitates effective stress transfer and enhances the electromechanical coupling within the composite.

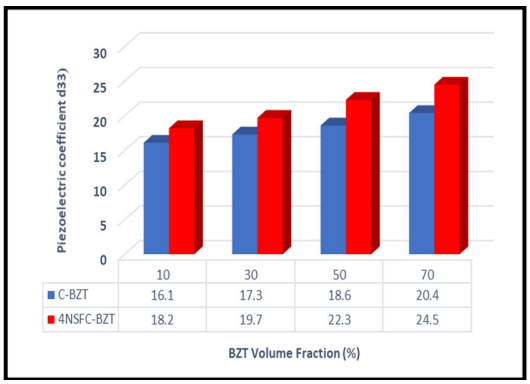

Fig. 11. Effect of BZT volume fractions on the piezoelectric coefficient of cement mortar with and without NSF.

F. Acoustic Impedance

Acoustic impedance is defined as the product of material density and sound velocity, and it is crucial for applications in ultrasonic sensing and structural health monitoring. Figure 12 illustrates the variation of acoustic impedance with BZT volume fraction for mortars with and without NSF.

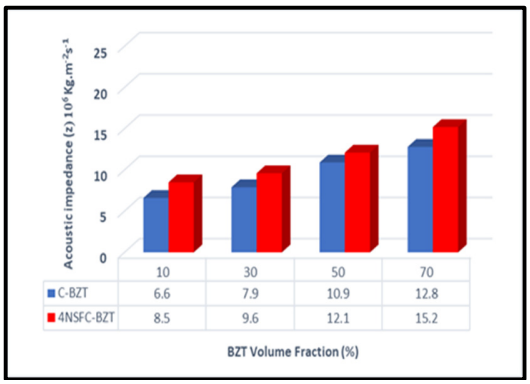

Fig. 12. Effect of BZT volume fractions on acoustic impedance of cement mortar with and without NSF.

The inclusion of BZT increased the acoustic impedance due to its higher density and stiffness relative to cement. The addition of NSF further improved this property by refining the microstructure, reducing porosity, and increasing sound velocity. NSF effectively minimized acoustic wave scattering by filling pores and strengthening the matrix, thereby enhancing impedance consistency.

The observed improvements in dielectric, piezoelectric, and acoustic properties are interrelated, arising from NSF-induced densification, reduced porosity, and improved particle–matrix interfaces, which together optimize the charge storage and stress transfer within the composite.

IV. CONCLUSIONS

The development of smart cementitious materials has become a central focus in structural health monitoring research. Previous studies have primarily emphasized carbon-based fillers for improving the electrical conductivity or nano-silica for enhancing the mechanical strength. However, the combined influence of nano-silica and lead-free piezoelectric ceramics, such as Barium Zirconate Titanate (BZT), on multifunctional mortar systems has been scarcely investigated.

In this study, BZT–cement mortar nano-composites incorporating Nano Silica Fume (NSF) were fabricated to explore the interaction between the mechanical and electrical performance. Unlike prior BZT–cement systems that addressed only electrical enhancement or nano-silica-modified mortars that targeted strength improvement, the present investigation demonstrates that the integration of NSF with BZT yields simultaneous enhancement in both the mechanical and functional properties.

Based on the experimental results, the following conclusions can be drawn:

- The SEM observations confirmed that the NSF addition refined the cement and composite microstructure, reducing voids and promoting matrix densification, which contributed to improved mechanical and functional performance.
- The nanoscale size and high pozzolanic reactivity of NSF facilitated its integration within the cement matrix and strengthened the interfacial interaction between the cement phases and BZT particles.
- An optimum NSF content was identified at 4 wt.%, beyond which the agglomeration effects became evident, leading to a reduction in mechanical strength.
- The inclusion of NSF improved the compressive strength through enhanced interfacial bonding, particle packing, and pore refinement, contributing to greater durability and crack resistance.
- The dielectric, piezoelectric, and acoustic properties of the composites increased proportionally with the BZT volume fraction embedded within the cement matrix.
- The dielectric constant of BZT-cement composites improved with NSF incorporation, indicating enhanced polarization and interfacial coupling.

- A reduction in dielectric loss was achieved in the presence of NSF due to improved microstructural uniformity and minimized electrical dissipation.
- The piezoelectric coefficient d_{33} exhibited a marked improvement as a result of a better BZT dispersion and enhanced domain alignment within the NSF-modified matrix.
- The acoustic impedance measurements revealed that composites containing 10-30 vol.% BZT achieved impedance values in the range of $(8.5\text{-}9.6)\times10^6$ $kg\cdot m^{-2}\cdot s^{-1}$, closely matching that of conventional concrete of 9×10^6 $kg\cdot m^{-2}\cdot s^{-1}$, indicating excellent compatibility for integration into smart concrete structures.

In summary, the incorporation of NSF into BZT-cement composites provides a synergistic enhancement of both the mechanical and electrical characteristics, establishing a sustainable, multifunctional material with strong potential for applications in intelligent infrastructure and structural health monitoring systems.

ACKNOWLEDGMENTS

The authors gratefully acknowledge the financial and technical support provided by Mustansiriyah University, College of Engineering, Baghdad, Iraq.

REFERENCES

[1] J. Ma *et al.*, "Composition, microstructure and electrical properties of $K_{0.5}Na_{0.5}NbO_3$ ceramics fabricated by cold sintering assisted sintering," *Journal of the European Ceramic Society*, vol. 39, no. 4, pp. 986–993, Apr. 2019, https://doi.org/10.1016/j.jeurceramsoc.2018.11.044.

[2] J. H. Kim *et al.*, "Preparation of CuO-doped (K,Na,Li)(Nb,Ta)O_3 ceramics with a homogeneous microstructure by Two-step sintering for multilayered piezoelectric energy harvesters," *Materials Letters*, vol. 241, pp. 202–205, Apr. 2019, https://doi.org/10.1016/j.matlet.2019.01.083.

[3] J. Hao, W. Li, J. Zhai, and H. Chen, "Progress in high-strain perovskite piezoelectric ceramics," *Materials Science and Engineering: R: Reports*, vol. 135, pp. 1–57, Jan. 2019, https://doi.org/10.1016/j.mser.2018.08.001.

[4] R. Huang, Y. Zhao, and D. Yan, "$(K_{0.5}Na_{0.5})NbO_3$ lead-free ceramics with improved piezoelectricity and field-induced strain," *Ceramics International*, vol. 45, no. 1, pp. 1450–1454, Jan. 2019, https://doi.org/10.1016/j.ceramint.2018.09.275.

[5] P. Li *et al.*, "High-performance potassium-sodium niobate lead-free piezoelectric ceramics based on polymorphic phase boundary and crystallographic texture," *Acta Materialia*, vol. 165, pp. 486–495, Feb. 2019, https://doi.org/10.1016/j.actamat.2018.12.024.

[6] W. Yang, P. Li, F. Li, X. Liu, B. Shen, and J. Zhai, "Enhanced piezoelectric performance and thermal stability of alkali niobate-based ceramics," *Ceramics International*, vol. 45, no. 2, Part A, pp. 2275–2280, Feb. 2019, https://doi.org/10.1016/j.ceramint.2018.10.141.

[7] Z. Dai *et al.*, "High piezoelectricity of $BiScO_3$-$PbTiO_3$ ceramics prepared by two step sintering," *Materials Letters*, vol. 241, pp. 55–59, Apr. 2019, https://doi.org/10.1016/j.matlet.2019.01.046.

[8] L. F. Zhu *et al.*, "Enhanced piezoelectric and ferroelectric properties of BiFeO3-BaTiO3 lead-free ceramics by optimizing the sintering temperature and dwell time," *Journal of the European Ceramic Society*, vol. 38, no. 10, pp. 3463–3471, Aug. 2018, https://doi.org/10.1016/j.jeurceramsoc.2018.03.044.

[9] R. Rianyoi, R. Potong, A. Ngamjarurojana, and A. Chaipanich, "Dielectric and piezoelectric properties of 2-2 connectivity lead-free piezoelectric ceramic $Bi_{0.5}Na_{0.5}TiO_3$/Portland cement composites," *Ceramics International*, vol. 44, pp. S220–S223, Nov. 2018, https://doi.org/10.1016/j.ceramint.2018.08.110.

[10] N. Jaitanong, S. Narksitipan, A. Ngamjarurojana, and A. Chaipanich, "Influence of graphene nanoplatelets on morphological and electrical properties of silica fume blended cement – Piezoelectric ceramic composite," *Ceramics International*, vol. 44, pp. S137–S140, Nov. 2018, https://doi.org/10.1016/j.ceramint.2018.08.131.

[11] R. Prasad, A. E. Mahmoud, and S. K. S. Parashar, "Enhancement of electromagnetic shielding and piezoelectric properties of White Portland cement by hydration time," *Construction and Building Materials*, vol. 204, pp. 20–27, Apr. 2019, https://doi.org/10.1016/j.conbuildmat.2019.01.140.

[12] N. Jaitanong, R. Yimnirun, H. R. Zeng, G. R. Li, Q. R. Yin, and A. Chaipanich, "Piezoelectric properties of cement based/PVDF/PZT composites," *Materials Letters*, vol. 130, pp. 146–149, Sep. 2014, https://doi.org/10.1016/j.matlet.2014.05.040.

[13] T. Wittinanon, R. Rianyoi, R. Potong, and A. Chaipanich, "Effect of epoxy resin addition on the acoustic impedance, microstructure, dielectric and piezoelectric properties of 1–3 connectivity lead-free barium zirconate titanate ceramic cement-based composites," *Ceramics International*, vol. 50, no. 23, Part C, pp. 52144–52151, Dec. 2024, https://doi.org/10.1016/j.ceramint.2024.10.251.

[14] P. Julphunthong, P. Wiwatrojanagul, P. Tiantong, T. Bongkarn, R. Rianyoi, and R. Potong, "Development and evaluation of KNLNTS-cement composites for use as piezoelectric sensors in structural health monitoring applications," *Results in Engineering*, vol. 25, Mar. 2025, Art. no. 104526, https://doi.org/10.1016/j.rineng.2025.104526.

[15] R. Potong, R. Rianyoi, A. Ngamjarurojana, and A. Chaipanich, "Dielectric and piezoelectric properties of 1–3 non-lead barium zirconate titanate-Portland cement composites," *Ceramics International*, vol. 39, pp. S53–S57, May 2013, https://doi.org/10.1016/j.ceramint.2012.10.034.

[16] P. Chomyen, R. Potong, R. Rianyoi, A. Ngamjarurojana, P. Chindaprasirt, and A. Chaipanich, "Microstructure, dielectric and piezoelectric properties of 0–3 lead free barium zirconate titanate ceramic-Portland fly ash cement composites," *Ceramics International*, vol. 44, no. 1, pp. 76–82, Jan. 2018, https://doi.org/10.1016/j.ceramint.2017.09.112.

[17] W. Ding, Y. Liu, T. Shiotani, Q. Wang, N. Han, and F. Xing, "Cement-Based Piezoelectric Ceramic Composites for Sensing Elements: A Comprehensive State-of-the-Art Review," *Sensors*, vol. 21, no. 9, Jan. 2021, Art. no. 3230, https://doi.org/10.3390/s21093230.

[18] C. Zhuang and Y. Chen, "The effect of nano-SiO_2 on concrete properties: a review," *Nanotechnology Reviews*, vol. 8, no. 1, pp. 562–572, Jan. 2019, https://doi.org/10.1515/ntrev-2019-0050.

[19] P. Brzozowski, J. Strzałkowski, P. Rychtowski, R. Wróbel, B. Tryba, and E. Horszczaruk, "Effect of Nano-SiO_2 on the Microstructure and Mechanical Properties of Concrete under High Temperature Conditions," *Materials*, vol. 15, no. 1, Jan. 2022, Art. no. 166, https://doi.org/10.3390/ma15010166.

[20] F. Huang *et al.*, "Impact of silica fume on the long-term stability of cement-based materials with low water-to-binder ratio under different curing conditions," *Construction and Building Materials*, vol. 450, Nov. 2024, Art. no. 138604, https://doi.org/10.1016/j.conbuildmat.2024.138604.

[21] H. M. Kamal, M. J. Kadhim, and R. K. M. Jawad, "Investigate the colloidal nano-zinc oxide addition on the strength acceleration of G-sand cement mortar," *AIP Conference Proceedings*, vol. 2213, no. 1, Mar. 2020, Art. no. 020148, https://doi.org/10.1063/5.0000294.

[22] "Standard Test Method for Density, Absorption, and Voids in Hardened Concrete," ASTM International, West Conshohocken, PA, Standard C642-21, Jan. 2022.

[23] M. J. Kadhim, L. M. Hasan, and H. M. Kamal, "Investigating the effects of nano-blast furnace slag powder on the behaviour of composite cement materials," *Journal of Achievements in Materials and Manufacturing Engineering*, vol. 116, no. 1, pp. 5–10, Jan. 2023, https://doi.org/10.5604/01.3001.0016.3392.

[24] M. F. Qasim, Z. K. Abbas, and S. K. Abed, "Producing Green Concrete with Plastic Waste and Nano Silica Sand," *Engineering, Technology &*

Applied Science Research, vol. 11, no. 6, pp. 7932–7937, Dec. 2021, https://doi.org/10.48084/etasr.4593.

[25] "Standard Test Method for Compressive Strength of Hydraulic Cement Mortars(Using 2-in. or [50-mm] Cube Specimens)," ASTM International, West Conshohocken, PA, Standard C109/C109M-05, Aug. 2017.

[26] C. Shi *et al.*, "Design and manufacture of lead-free eco-friendly cement-based piezoelectric composites achieving superior piezoelectric properties for concrete structure applications," *Composites Part B: Engineering*, vol. 259, Jun. 2023, Art. no. 110750, https://doi.org/10.1016/j.compositesb.2023.110750.